# Evidence of near-the-limit energy cost NO formation in atmospheric spark discharge

Nikolay Britun[1], Vladislav Gamaleev[1,2], Masaru Hori[1]
[1] *Center for Low-temperature Plasma Sciences, Nagoya University, Chikusa-ku, 464-8603 Nagoya, Japan and*
[2] *The present address: Air Liquide Laboratories, 2-2 Hikarinooka, 239-0847 Yokosuka, Japan*

We report a very low energy cost for NO radical formation found in atmospheric spark discharge. For this purpose non-equilibrium air discharges working in spark and glow regimes were studied showing the optimum performance in the vicinity of the spark-to-glow transition. The minimum energy cost for NO production of about 80 eV/molecule (calculated based on the *total* direct current power applied to the discharge) is achieved in the spark regime before the transition, whereas the maximum NO yield (of about $10^4$ part per million) corresponds to the glow regime. Based on the estimated power *absorbed in plasma* the energy cost below 4 eV/molecule is achievable in the spark regime, which is close to the Zeldovich reaction enthalpy of NO formation (about 3 eV/molecule). The result implies that the energetic efficiency of a single spark likely exceeds that of the modern Haber-Bosch cycle (with energy cost of about 5 eV/molecule in the case of ammonia, according to Patil *et al.*, Catalysis Today, **256** (2015) 49). The found low energy cost is associated with the discharge non-equilibrium caused by short spark duration.

*Keywords:* Nitric oxide, nitrogen fixation, energy cost, atmospheric discharge, sparks, non-equilibrium.
PACS numbers: 52.20.-j, 52.25.Ya, 52.38.Dx, 52.70.-m, 82.33.Xj, 84.60.-h

Ecologically friendly production of the N- containing compounds at the atmospheric conditions is of a great importance, which is dictated by the abundance of (hard to dissociate) molecular nitrogen in the atmosphere and by the necessity to replace the existing Haber-Bosch process. The latter process is used for N- containing compound production since the beginning of XX-th century featuring high energy consumption and high $CO_2$ emission [1, 2] which still should be overcome.

Low-temperature discharges are considered as a suitable alternative for N- compounds production, due to the high chemical reactivity resulted by a non-equilibrium between the electrons and heavy particles [3]. Vibrational excitation of molecular species may additionally reduce the energy barriers for the key processes in these discharges, such as dissociation [4].

Energy cost (EC) for a single molecule production is defined as a ratio between the energy spent and the number of particles generated, which also can be expressed via the applied power and the gas flow (see supplementary data 1):

$$EC \approx 1.4 \cdot 10^4 \cdot P/(\gamma F), \qquad (1)$$

here EC is in eV per molecule (eV/mlc notation is used below), $P$ is the applied power (in W), $\gamma$ is the production yield (in part per million, ppm), $F$ is the total gas flow (in standard liter per minute, slm).

Atmospheric pressure discharges play special role in gas reforming since they may convert industrial gas mixtures without additional pressure reduction. The EC values for $NO_x$ production typically less than 100 eV/mlc have been reported in the atmospheric spark (53 eV/mlc), propellor-arc (37 eV/mlc) [5] and glow (36 eV/mlc) [6] discharges. It is also known that the atmospheric spark discharge reveals lower EC values of $NO_x$ production (89 eV/mlc) [7] than those found in spark-glow mixtures [8]. What is related to NO generation, rather close values were found in spark (< 100 eV/mlc) [9], rotating glow (78 eV/mlc) [10] and coaxial plasmatron (35 eV/mlc) [11] discharges, including the particular cases of spark (≈ 20 eV/mlc, found only at the end of plasma pulse) [5] and atmospheric arc (≈ 16 eV/mlc) [12] discharges.

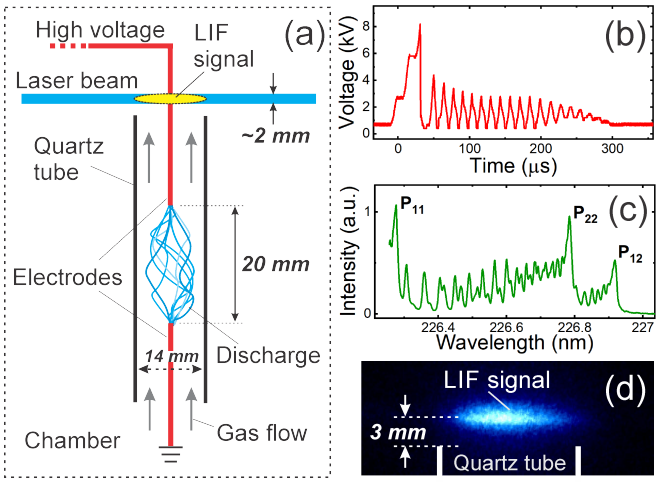


FIG. 1. The discharge schematics (a), voltage re-pulsations in a single plasma cycle in the glow regime (b), laser-absorption spectrum of the NO $^2\Sigma^+(v'=0) \leftarrow {}^2\Pi(v''=0)$ transition (c) and the appearance of LIF signal in the reactor (d).

NO radical production in plasma is often associated with so called Zeldovich mechanism [1, 3]: $N_2(X,v)$+O → NO+N (R1), $O_2(X,v)$+N → NO+O (R2) where vibrationally excited molecules ($v$) are of a great importance. The reaction R1 normally dominates, as $O_2$ is easier to dissociate. Apart from the electron impact dissociation, $O_2$ photolysis, $O_2+h\nu \rightarrow O+O$ (R3), may also

play important role in O atom production, especially in spark discharges [9]. In low pressure non-equilibrium plasma energy cost of NO production can be as low as the enthalpy of Zeldovich reaction R1 ($\Delta H \approx 3\,\mathrm{eV/mlc}$) [4, 13], whereas in the atmospheric air discharges the question about reaching this limit remains opened.

In this Letter we demonstrate the benefits of using spark-to-glow transition in atmospheric air discharge for energetically efficient NO production. The plasma system where discharge can operate in corona, spark, subnormal and normal glow regimes has been utilized (Fig. 1(a)). The discharge regimes listed above have already been revealed in the previous studies [14, 15].

A custom generator consisting of a regulated direct current (DC) power supply, push-pull generator with pulse width modulation (PWM), diode rectifier and reservoir capacitor has been implemented [16]. The use of PWM assured enhanced discharge control and plasma stability at higher gas flows [17]. The discharge has been sustained between two Cu electrodes (2 mm in diameter) in a quartz tube with 14 mm inner diameter and 10 cm height (in the upcoming dry air flow). The system was placed into a sealed chamber with sub-atmosphere pressure ($\approx 0.95$ bar). The corresponding electrical circuitry is available in supplementary data 2.

In the glow regime the plasma is defined by PWM process leading to voltage re-pulsations within each plasma-on time (see Fig. 1(b)). In the spark regime the plasma is represented by short ($\approx 20$ ns) events randomly distributed in time. The spark rate measured at 1 kHz of PWM frequency and 10W of DC power gives $240 \pm 40$ spark/s (see supplementary data 3), which is consistent with previous studies [15].

The optical transition between two NO electronic states, $^2\Sigma^+(v'=0) \leftarrow {}^2\Pi_{3/2}(v''=0)$, is exploited for NO ground state density detection using laser-induced fluorescence (LIF) spectroscopy. A dye laser pumped by a pulsed YAG:Nd laser (with 10 ns pulse duration) has been used for excitation. The NO $^2\Pi_{3/2}(v''=0)$ ground state has been excited at $\approx 226.87$ nm corresponding to the rotational bandhead of the $P_{22}$ branch [18]. The laser wavelength has been fixed based on the laser-absorption spectrum of NO recorded prior to measurements (Fig. 1(c)). The LIF signal has been measured 3 mm above the discharge tube (see Fig. 1(d)) by acquiring the entire $^2\Sigma^+(v'=0) \rightarrow {}^2\Pi(v''=2)$ NO emission band using an intensified charge coupled device (ICCD) synchronized with the laser system (for details see supplementary data 4).

The density ($n_j$) of species in the ground state ($j$) detected using single photon excitation process involving fluorescence between the excited ($i$) and intermediate ($k$) electronic states reads [19, 20]:

$$n_j = C \frac{I_{fluor}}{I_{las}} \frac{(A_i + Q_i)}{h\nu_{ik} A_{ik} B_{ji}}, \qquad (2)$$

where $C$ is a constant, $I_{fluor}$ and $I_{las}$ are the fluorescence and the laser beam intensity, $A_i$ and $Q_i$ are the

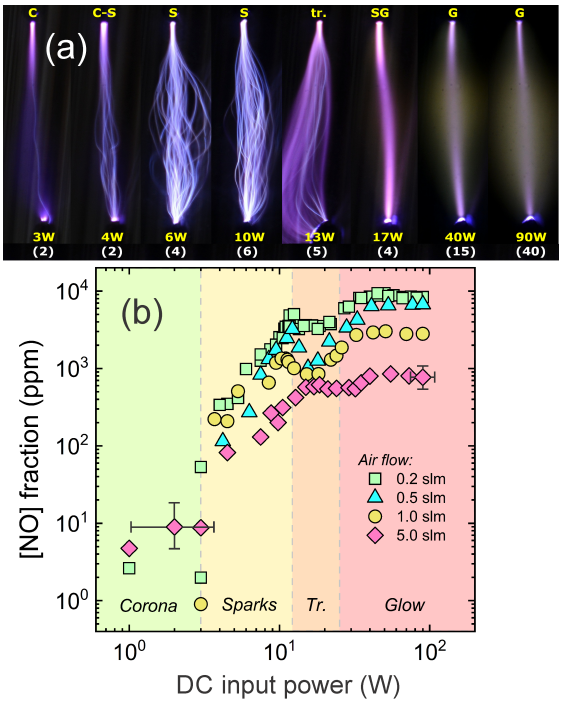


FIG. 2. The discharge photographs (a) and NO fraction produced (b) as a function of DC input power. The following abbreviations are used: C- corona, C-S- corona-sparks, S- sparks, Tr.- transition, SG- sub-normal glow, G- normal glow. Camera exposure values (in $\mathrm{s}^{-1}$) are parenthesized in the (a) case. Typical error bars are given for corona and glow regimes.

radiative and quenching losses in the ($i$) state, $h$ is the Planck's constant, $\nu_{ik}$ is the frequency of the fluorescence photons, $A_{ik}$ is the spontaneous emission coefficient for $i \rightarrow k$ transition, $B_{ji}$ is the absorption coefficient for $j \rightarrow i$ transition. In our case $I_{fluor} \propto I_{las}^x$, with $x = 1.01$, corresponding to a non-saturated LIF case.

The NO number density has been calibrated in Ar/NO gas mixture without plasma where the fluorescence scales linearly with NO admixture (fitting error $< 2\%$). A ratio of the NO ground state populations in the air and Ar cases, based on Eq. (2), yields:

$$n = n^0 \cdot \frac{I_{LIF}}{I^0_{LIF}} \cdot \frac{A_i + Q_i}{A^0_i + Q^0_i} = n^0 \cdot \frac{I_{LIF}}{I^0_{LIF}} \cdot \frac{\tau^0}{\tau}, \qquad (3)$$

where $n$ denotes number density, "0" superscript corresponds to the Ar case (calibration), $I_{LIF} \equiv I_{fluor}/I_{las}$, $\tau$ is the effective lifetime of the $i$ state limited by collisional quenching and radiative losses.

The quenching coefficients were carefully compared in the air and Ar cases. Since the quenching of NO by Ar is not well defined in literature [21], the lifetime of the $^2\Sigma^+(v'=0)$ state has been measured directly giving $21.5 \pm 3.9$ ns. In dry air the main NO quencher is $O_2$ [22–24] giving the corresponding lifetime of $1.09 \pm 0.03$ ns (not measurable due to the long laser pulse in our case). The $A_i$ was neglected as it is nearly two orders of magnitude smaller than $Q_i$ [25]. The gas temperature ($T_{gas}$)

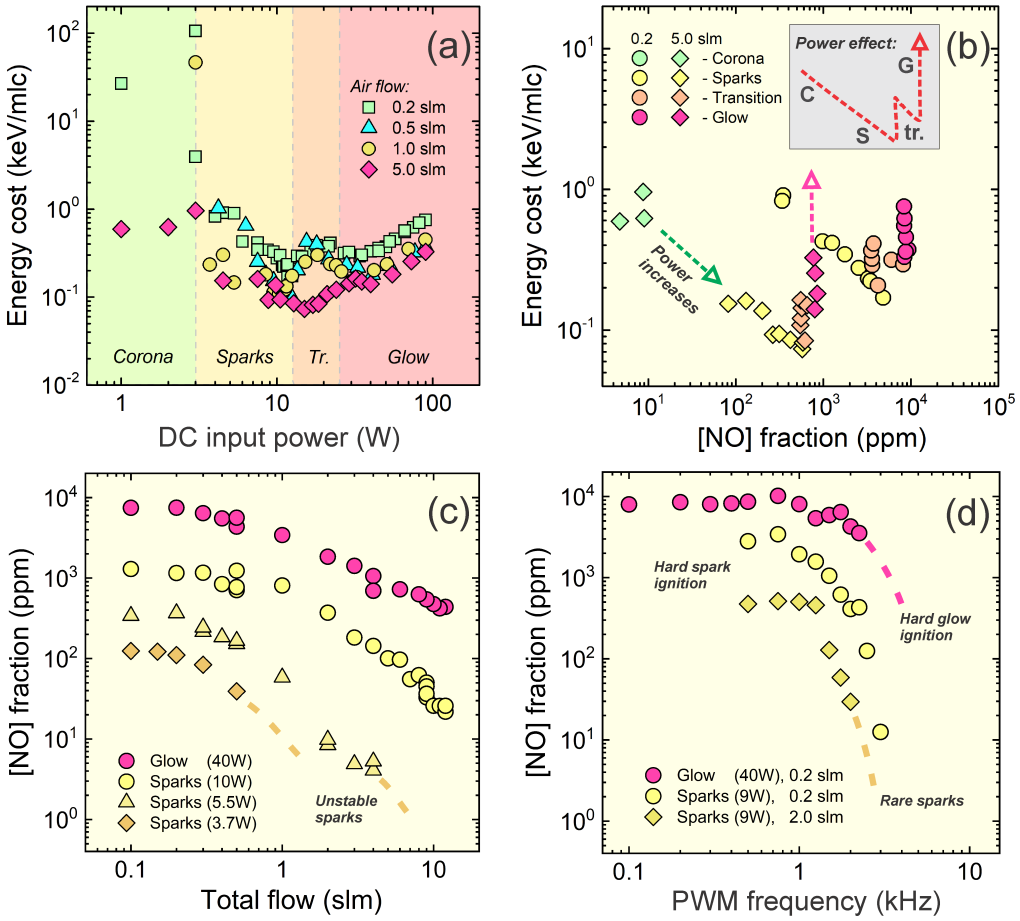


FIG. 3. The discharge performance presented in the coordinates EC - input power (a) and EC - NO fraction (b), NO fraction - total flow (c) and NO fraction - PWM frequency (d). The Energy cost - NO production routes are sketched in the inset of (b) panel (for abbreviations refer to the caption of Fig. 2).

above the quartz tube is assumed equal to 300 K based on the gas thermalization time measured at low pressure [26]; this leads to a fixed relative populations of the $^2\Pi_{1/2}$ and $^2\Pi_{3/2}$ states of NO. If this assumption breaks the contribution of the lower state ($^2\Pi_{1/2}$) decreases resulting in overestimation of total ground state density. In the Boltzmann approximation, the density overestimation may be about 10 % at $T_{gas}$ is 400 K and as high as 15 % if $T_{gas}$ reaches 500 K.

We found that both the discharge appearance (Fig. 2(a)) and the NO production (Fig. 2(b)) evolve dramatically as a result of DC power increase: the corona regime, spark regime, transition interval, subnormal and normal glow regimes are clearly observable. The discharge emission is mainly composed by the $N_2$, NO and OH ro-vibrational bands with last two being much more pronounced in the glow regime (see supplementary data 5).

The measured NO fraction covers nearly 4 orders of magnitude in our case (Fig. 2(b)) being vanishingly small in the corona case, rapidly increasing afterwards and saturating in the glow regime. As a result of the discharge instabilities in the corona regime, the applied discharge power, the corona-spark boundary as well as the NO fraction itself are poorly defined (error is roughly 50 %). The NO fraction reveals local maximum before the transition point (at about 10 W, 0.2 slm), corresponding to efficient coverage of the gas volume by sparks (Fig. 2(a)) and possessing low energy cost (see Fig. 3). The error of the NO fraction in the late spark, transition and glow regimes is mainly defined by the laser energy variations (roughly 10% from the mean value). The calibration procedure induces additional error which is defined by the gas flow controllers (about 10%). The net error for the NO fraction based on Eq. (3) estimated using so-called square root sum method [27] taking into account both the laser and calibration errors is about 17 % in our case.

At low gas flow EC drops by about 3 orders of magnitude (compared to corona case) reaching a minimum before the spark-to-glow transition (in Fig. 3(a) the transition point is somewhat shifted toward the higher power values at high gas flow). Looking at these data in the NO fraction - EC coordinates (Fig. 3(b)) we can see that, after the first minimum (spark regime), EC grows rapidly

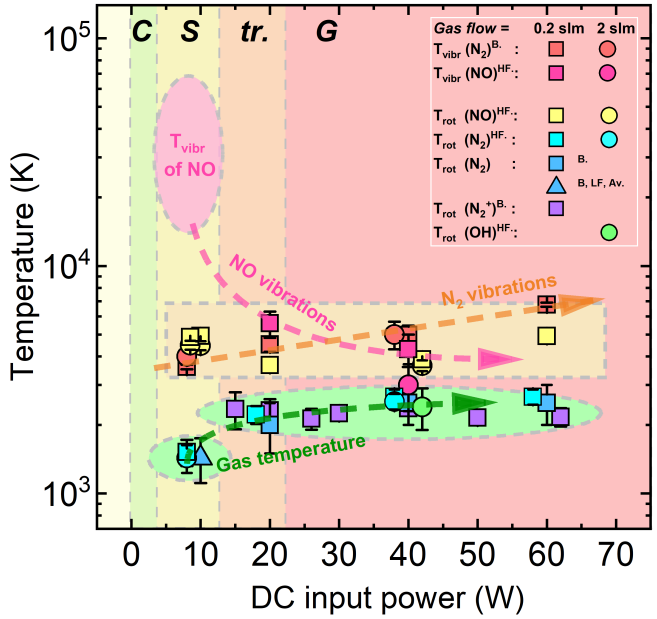


FIG. 4. Summary of vibrational and rotational temperatures measured in the discharge core using several molecular excited states, such as $N_2$ $C\,^3\Pi_u$, NO $A\,^2\Sigma^+$, OH $A\,^2\Sigma^+$ and $N_2^+$ $B\,^2\Sigma_u^+$. (In the legend B, HF, LF, and Av. symbols denote Boltzmann plot, high-resolution fitting, low-resolution fitting, and average value for both gas flows, respectively).

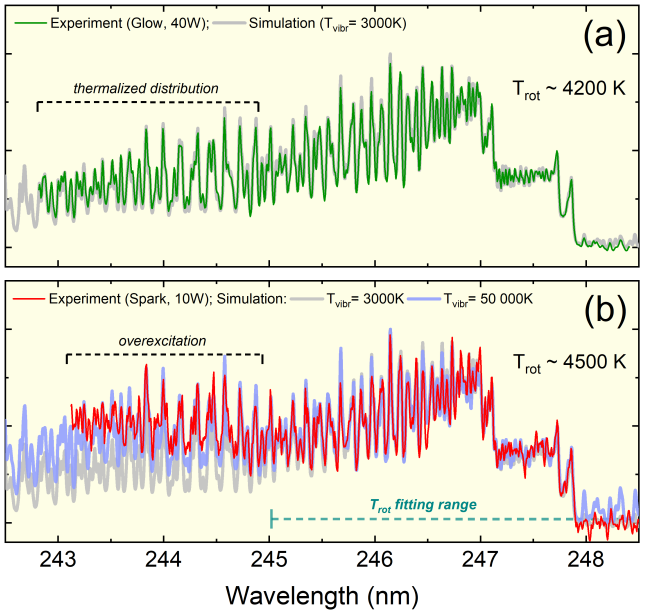


FIG. 5. Normalized NO ($A^2\Sigma^+ \rightarrow X^2\Pi$ (0,2)) emission spectra in the glow (a) and spark (b) regime. Gas flow is 0.2 slm. Single temperature fit reveals a nearly perfect thermalization in the glow case whereas an overexcited tail is clear in the spark case. The same band corresponding to different $T_{vibr}$ is shown for reference. Spectral resolution is about 30 pm.

during the transition interval showing no increase in the NO production and, after a little decrease, retains its (vertical) growth in the glow regime. All in all, a clear W-shape is formed for each gas flow value (see inset in Fig. 3(b)). The minimum EC value of about 80 eV/mlc is found (at 5 slm of the total gas flow). The second minimum at the beginning of the glow regime has roughly twice higher EC and, thus, not beneficial energetically.

The NO fraction is also strongly affected by the gas flow and the PWM frequency (see Fig. 3(c,d)). Remaining stable at low gas flow ($< 0.3$ slm), it slowly decreases afterwards. At high gas flow sparks reveal instabilities likely induced by gas turbulence increasing the breakdown voltage. The NO fraction also drops considerably when frequency is $> 1$ kHz (Fig. 3(d)). At low frequency sparks become hard to ignite due to the low residual ion density at longer plasma-off time, which is not enough for stable plasma ignition. Also, when plasma-on time is shorter than the reservoir capacitor charging time (frequency is $> 2$ kHz) [16], both glow and sparks reveal hard ignition (Fig. 3(d)).

Physical mechanisms behind the found trends can be clarified after a detailed consideration of ro-vibrational excitation in the discharge. The rotational ($T_{rot}$) and vibrational ($T_{vibr}$) temperature data measured during the plasma-on time clearly indicate the presence of non-equilibrium in the discharge core: $T_{vibr}^{N_2} \geq T_{rot}^{NO} > T_{gas}$ in the glow case (see Fig. 4). In this case the rotational spectra were fitted using a specially developed code based on simulated datasets. The simulated spectra were synthesized using LIFBASE software (v 2.1.1) [28]. The temperature error is defined by a simulation step, which was equal to 100 K in most cases. By additional fitting of the behavior of spectral residuals the final temperature error has been further reduced in each case. For the $T_{vibr}^{N_2}$ the Boltzmann fitting error is used as the final temperature uncertainty.

In Fig. 4 $T_{gas}$ is associated with the value of about 2000-2500 K since it corresponds to rotational equilibrium between numerous molecules. The found gas temperature values agree well with the previous works dealing with glow discharges [29, 30]. $T_{vibr}^{N_2}$ gradually increases with the applied power, whereas $T_{rot}^{NO}$ is roughly about 4000 K. The obtained $T_{vibr}$ values in the glow regime (5000-7000K) exceeds the ones found in the DC glow previously [30], however, maintaining a jump toward the lower $T_{vibr}$ in the spark regime ($T_{vibr}$ is about 3500 K in our case). The proximity of $T_{vibr}^{N_2}$ and $T_{rot}^{NO}$ in both glow and sparks cases points out the importance of the vibrational channel for NO excitation, in addition to translational-rotational (T-R) exchange.

Spark regime reveals higher degree of non-equilibrium: $T_{gas}$ is lower in this case ($\approx$1400 K, see supplementary data 6), whereas $T_{rot}^{NO}$ increases up to about 4500 K. Much lower gas temperature (no higher than 600 K) in a pure transient 100 ns spark regime has been reported by Machala *et al.* [30], which, together with our results contradict with a fast gas heating found by Pai *et al.* [15] where gas temperature elevation up to several thousands K during 30 ns spark has been measured. Only one ($N_2$)

rotational emission band has been used for $T_{rot}$ in the last case, though.

Low gas temperature observed in the spark regime in this work should likely be associated with slow vibrational-vibrational (V-V) and vibrational-translational (V-T) energy transfer. Based on the available data [31], the estimated time constants for these processes in the nitrogen case are equal to at least few hundred ns (V-V) and few $\mu$s (V-T), which are much longer than the spark duration. The suggested non-equilibrium strongly corroborates with the measured rotational spectra of NO showing thermal distribution in the glow case (with $T_{vibr}$ of NO $\approx 3000\,K$) but having a clear non-thermal shape in the spark case (see Fig. 5). Thus, high vibrational excitation of NO possibly possessing a Treanor-like [32] distribution may be suggested for the spark regime. We could not localize the value for $T_{vibr}$ for NO solely based on spectra fitting, however, its lower limit we believe is roughly $10^4\,K$.

The reactions R1 and (to a less extent) R2 likely assisted by $O_2$ photolysis (R3) [9] represent the most probable pathway for NO generation in the spark regime. In the glow regime higher vibrational excitation may additionally increase $N_2$ dissociation (e.g. via $N_2 + N_2(X, v = 45) \rightarrow N_2 + N + N$ [33]). The other processes, such as dissociative recombination ($e^- + N_2^+ \rightarrow N + N$) may also be important, as supported by the presence of $N_2^+$ rotational emission band in glow regime in our case, which is absent in sparks.

The EC values given in Fig. 3 are based on the *total* DC input power applied to the plasma system. The fraction of this power absorbed in the glow plasma is $\eta \approx 41\,\%$, whereas the power fraction absorbed by sparks in only $\eta \approx 4.3 \pm 0.8\%$. The energy absorbed solely by sparks is calculated as a product of a single spark energy (based on the current-voltage waveform integration) to the spark repetition rate. The (small) amount of NO produced by corona discharges appearing between the spark events is normally negligible, as corona discharge possesses very small currents (mA range) as compared to the spark currents (20 A typically), so the power is mainly channelized to sparks.

In terms of the spark- absorbed power ($P_{abs} = \eta P$) the minimum EC found in this work ($\approx 80\,eV/mlc$) corresponds to only about $3.5 \pm 0.7\,eV/mlc$, according to Eq. (1). This energy is very close to the enthalpy $\Delta H$ of the Zeldovich reaction R1, at the same time lying below the value for the industrial Haber-Bosch cycle [1]. The corresponding NO production rate is about $1.5 \cdot 10^{18}\,s^{-1}$, which is still one order of magnitude lower than the value found in Ar- dominated atmospheric jet [34].

The comparable energy cost has only been found so far in the low pressure microwave discharges without [4] and with catalysis [13], or in Ar plasma jet [34]. In the atmospheric air spark discharge [9] the noticeably higher EC values were observed, most likely because of intensive gas heating. Another reason for underestimated efficiency of spark discharges in the literature may be a poor spark rate estimations. By contrast, the low EC obtained in our case is related to the combination of high electron and vibrational excitation, contribution of photolysis, and low gas heating provided by ns-scale spark duration.

Concluding, a spark discharge possessing vibrational-translational non-equilibrium allows efficient NO radical generation at a near-the-limit energy cost. In order to increase NO production yield the additional challenges, such as increasing of spark repetition and density as well as elimination of extra power losses, should be overcome by further discharge modifications, including better volume coverage at higher spark rates.

This work is supported by JSPS KAKENHI (grant 19H05462). We also thank PhD student Omid Samadi (Mons University, Belgium) for $N_2$ spectra synthesis.

[1] B. Patil, Q. Wang, V. Hessel, and J. Lang, Catalysis Today **256**, 49 (2015).
[2] N. Cherkasov, A. Ibhadon, and P. Fitzpatrick, Chemical Engineering and Processing: Process Intensification **90**, 24 (2015).
[3] A. A. Fridman, *Plasma Chemistry* (Cambridge University Press, Cambridge, 2005).
[4] V. D. Rusanov, A. A. Fridman, and G. V. Sholin, Uspekhi Fiz. Nauk **134**, 185 (1981).
[5] X. Pei, D. Gidon, Y.-J. Yang, Z. Xiong, and D. B. Graves, Chemical Engineering Journal **362**, 217 (2019).
[6] X. Pei, D. Gidon, and D. B. Graves, Journal of Physics D: Applied Physics **53**, 044002 (2020).
[7] M. Janda, V. Martišovitš, K. Hensel, and Z. Machala, Plasma Chemistry and Plasma Processing **36**, 767 (2016).
[8] M. J. Pavlovich, T. Ono, C. Galleher, B. Curtis, D. S. Clark, Z. Machala, and D. B. Graves, **47**, 505202 (2014).
[9] V. Shmelev, A. Saveliev, and L. Kennedy, Plasma Chemistry and Plasma Processing **29**, 275 (2009).
[10] V. Gamaleev, N. Iwata, M. Hiramatsu, and M. Ito, Japanese Journal of Applied Physics **59**, SHHF04 (2020).
[11] Y. Korolev, O. Frants, N. Landl, and A. Suslov, IEEE transactions on plasma science **40**, 2837 (2012).
[12] Y. Wang, A. W. DeSilva, G. C. Goldenbaum, and R. R. Dickerson, Journal of Geophysical Research: Atmospheres **103**, 19149 (1998).
[13] B. Mutel, O. Dessaux, and P. Goudmand, Revue de Physique Appliquee **19**, 461 (1984).
[14] D. Z. Pai, G. D. Stancu, D. A. Lacoste, and C. O. Laux, Plasma Sources Science and Technology **18**, 045030 (2009).
[15] D. Z. Pai, D. A. Lacoste, and C. O. Laux, Plasma Sources Science and Technology **19**, 065015 (2010).
[16] V. Gamaleev, N. Britun, and M. Hori, IEEE Access **8**, 201486 (2020).
[17] V. Gamaleev, T. Tsutsumi, M. Hiramatsu, M. Ito, and M. Hori, IEEE Access **8**, 72607 (2020).

[18] J. Danielak, U. Domin, R. Kepa, M. Rytel, and M. Zachwieja, Journal of Molecular Spectroscopy **181**, 394 (1997).
[19] G. Kirkbright and M. Sargent, *Atomic Absorption and Fluorescence Spectroscopy*, 1st ed. (Academic Press, London, 1974).
[20] N. Britun and J. Hnilica, Journal of Applied Physics **127**, 211101 (2020).
[21] J. Few and G. Hancock, Phys. Chem. Chem. Phys. **16**, 11047 (2014).
[22] P. Paul, J. Gray, J. Durant Jr., and J. Thoman Jr., Chemical Physics Letters **259**, 508 (1996).
[23] T. B. Settersten, B. D. Patterson, and J. A. Gray, The Journal of Chemical Physics **124**, 234308 (2006).
[24] T. B. Settersten, B. D. Patterson, and C. D. Carter, The Journal of Chemical Physics **130**, 204302 (2009).
[25] T. B. Settersten, B. D. Patterson, and W. H. Humphries, The Journal of Chemical Physics **131**, 104309 (2009).
[26] J. Hnilica, P. Klein, P. Vašina, R. Snyders, and N. Britun, Journal of Applied Physics **128**, 043303 (2020).
[27] G. Rabinovich, *Evaluating Measurement Accuracy: A Practical Approach* (Springer, New York, 2010).
[28] J. Luque and D. Crosley, LIFBASE: Database and Spectral Simulation Program (Version 2.1.1) (1999).
[29] S. Huang, T. Li, Z. Zhang, and P. Ma, Applied Energy **251**, 113358 (2019).
[30] Z. Machala, M. Janda, K. Hensel, I. Jedlovský, L. Leštinská, V. Foltin, V. Martišovitš, and M. Morvová, Journal of Molecular Spectroscopy **243**, 194 (2007).
[31] L. Terraz, T. Silva, A. Morillo-Candas, O. Guaitella, A. T. del Caz, L. L. Alves, and V. Guerra, Journal of Physics D: Applied Physics **53**, 094002 (2019).
[32] C. E. Treanor, J. W. Rich, and R. G. Rehm, The Journal of Chemical Physics **48**, 1798 (1968).
[33] V. Guerra, E. Tatarova, F. M. Dias, and C. M. Ferreira, Journal of Applied Physics **91**, 2648 (2002).
[34] A. V. Pipa, T. Bindemann, R. Foest, E. Kindel, J. Röpcke, and K.-D. Weltmann, Journal of Physics D: Applied Physics **41**, 194011 (2008).